Self-consistent charge and dipole density functional tight binding method and application to carbon-based systems

Ying Wu[a,b], Adelina Ilie[a,b], Simon Crampin[a,b]

[a] *Department of Physics, University of Bath, Bath BA2 7AY, United Kingdom*
[b] *Centre for Graphene Science, University of Bath, Bath BA2 7AY, United Kingdom*

Abstract

The density functional tight binding (DFTB) method is a fast, semi-empirical, total energy electronic structure method based upon and parameterized to density functional theory (DFT). The standard self-consistent charge (SCC) DFTB approximates the charge fluctuations in a system using a multipole expansion truncated to the monopole term. For systems with asymmetric charge distributions, such as might be induced by an applied external field, higher terms in the multipole expansion are likely to be important. We have extended the formalism to include dipoles (SCCD), have implemented the method computationally, and test it by calculating the response of various carbon nanotubes and fullerenes to an applied electric field. A comparison of polarizabilities with experimental data or more sophisticated DFT calculations indicates a substantial improvement over standard SCC-DFTB. We also discuss the issues surrounding parameterization of the new SCCD-DFTB scheme.

Keywords: dipole, DFTB, DFT, tight-binding

1. Introduction

To accurately calculate the electronic structure of solid state materials, the density functional theory (DFT) has proven to be a trustworthy method if used appropriately. However, for large systems DFT is increasingly expensive. For these systems, a much faster semi-empirical method based upon the DFT framework, density func-

* Corresponding author
Email address: y.wu@bath.ac.uk (Ying Wu)

tional tight binding (DFTB) method [1; 2], can provide insight into the physical properties with a balance of accuracy and efficiency. First generation DFTB [1] approximates the total energy as a sum of the eigenvalues of all occupied states (also known as band structure energy) and a two-body repulsive energy, which is fitted to full DFT results. With careful parametrization, this method yields insightful structural and band structure results of various systems [1] possessing relatively small charge redistribution. Elstner et al. [2] extended the method to accommodate systems with considerable charge redistribution by introducing a charge fluctuation determined self-consistently to minimize the total energy. This method, self-consistent-charge-DFTB (SCC-DFTB), fundamentally enables the treatment of charge redistribution, and exhibits better results and transferability [2; 3]. Further extension of the DFTB framework are possible, e.g. as described in Ref [4].

Standard SCC-DFTB truncates the charge fluctuation around each atom to the monopole term. For systems with significantly asymmetrical charge distributions it is natural to consider achieving greater accuracy by extending the monopole approximation to higher terms. Bodrog and Aradi [4] have proposed using tabulated multipole interaction matrices and discussed formally some of the consequences for computation of the Hamiltonian and total energy. The specific method yielding the multipole interaction matrix and the parameterization have not been presented, nor implemented or applied. Motivated by a need to model with low cost large-scale graphene/graphitic films under the influence of external fields acting on the nanoscale, we develop the extension of the standard second-order DFTB framework to dipole terms proposed in [4]. We describe and implement a method to construct and tabulate the multipole interaction matrix, discuss parameterization issues, and validate and assess the dipole extension for carbon-based systems.

2. Self-consistent charge DFTB

First, we briefly summarize the theoretical background of SCC-DFTB. From DFT theory and the Kohn-Sham ansatz [5], the charge density $n(\mathbf{r})$ in the SCC-DFTB scheme [2] is expressed as a superposition of a reference density $n_0(\mathbf{r})$ and small

charge fluctuation $\delta n(\mathbf{r})$. The total energy is

$$\begin{aligned} E[n] = \sum_k f_k \langle \Psi_k | \left(-\frac{\nabla^2}{2} + \hat{V}_{\text{ext}} + \int d\mathbf{r}' \frac{n_0(\mathbf{r}') + \delta n(\mathbf{r}')}{|\mathbf{r} - \mathbf{r}'|} + V_{\text{xc}}[n_0 + \delta n] \right) | \Psi_k \rangle \\ - E_{\text{H}}[n_0 + \delta n] + E_{\text{xc}}[n_0 + \delta n] - \int d\mathbf{r} V_{\text{xc}}[n_0 + \delta n](n_0(\mathbf{r}) + \delta n(\mathbf{r})) + E_{\text{II}}, \end{aligned} \tag{1}$$

where f_k is the Fermi-Dirac occupation function of the state k, and Ψ_k is the corresponding single-particle wave function. $\hat{V}_{\text{ext}}$ describes the nuclear potential acting on the electrons, $\hat{V}_{\text{H}}[n]$ is the Hartree potential and $\hat{V}_{\text{xc}}[n]$ is the exchange-correlation potential. $E_{\text{H}}[n]$ is the Hartree energy, E_{II} the nuclear-nuclear Coulomb energy and $E_{\text{xc}}[n]$ the exchange-correlation energy. Writing the Kohn-Sham Hamiltonian as $\hat{H} = \hat{H}_0 + \left(\hat{H} - \hat{H}_0\right)$, where $\hat{H}_0$ refers to the system of reference charge density n_0, and expanding $E_{\text{xc}}[n_0 + \delta n]$ as a Taylor series gives the energy to second order in $\delta n(\mathbf{r})$

$$\begin{aligned} E[n] \approx & \sum_k f_k \langle \Psi_k | \hat{H}_0 | \Psi_k \rangle \\ & + \frac{1}{2} \int d\mathbf{r} \int d\mathbf{r}' \left(\frac{1}{|\mathbf{r} - \mathbf{r}'|} + \frac{\delta^2 E_{\text{xc}}[n]}{\delta n(\mathbf{r}) \delta n(\mathbf{r}')} \bigg|_{n_0(\mathbf{r}), n_0(\mathbf{r}')} \right) \delta n(\mathbf{r}') \delta n(\mathbf{r}) \\ & - \int d\mathbf{r} V_{\text{xc}}[n_0] n_0(\mathbf{r}) - \frac{1}{2} \int d\mathbf{r} \int d\mathbf{r}' \frac{n_0(\mathbf{r}) n_0(\mathbf{r}')}{|\mathbf{r} - \mathbf{r}'|} + E_{\text{xc}}[n_0] + E_{\text{II}}. \end{aligned} \tag{2}$$

The total energy comprises band structure energy E_{BS} (first term), second order energy E_{2nd} (second term) and the repulsive energy E_{rep}(remainder). The repulsive energy E_{rep} is approximately expressed as a sum of pair potentials that are a function of the distance between atoms i and j, $V_{\text{rep}}^{i,j}(R)$, the form of which is obtained by fitting to full DFT calculations [1; 2; 6]

$$E_{\text{rep}} = \sum_{i,j>i} V_{\text{rep}}^{i,j}(R) = \sum_{i,j>i} \left(E_{\text{DFT}}^{i,j}(R) - E_{\text{el}}^{i,j}(R) \right) \tag{3}$$

where E_{el} is the DFTB total energy without repulsive term. The band structure energy contains no contribution from charge fluctuations, with the Hamiltonian $\hat{H}_0$ determined by the reference charge density $n_0(\mathbf{r})$, which in the DFTB scheme is constructed as a sum of atomic charge densities. Correspondingly, single-particle wave

functions are expanded as linear combinations of atomic orbitals $\varphi_\mu(\mathbf{r})$,

$$\Psi_k(\mathbf{r}) = \sum_\mu c_\mu^k \varphi_\mu(\mathbf{r}). \tag{4}$$

where $\varphi_\mu(\mathbf{r}) = \varphi_\alpha(\mathbf{r} - \mathbf{R}_i)$ and composite index $\mu = (\alpha, i)$ distinguishes orbital α on atom i at $\mathbf{R}_i$. The band structure energy is

$$E_{\mathrm{BS}} = \sum_k f_k \langle \Psi_k | \hat{H}_0 | \Psi_k \rangle = \sum_k f_k \sum_\mu \sum_\nu c_\mu^{k*} c_\nu^k H_{\mu\nu}^0. \tag{5}$$

Composite indices $\mu = (\alpha, i), \nu = (\beta, j)$ are used throughout the text below.

The atomic orbitals $\varphi_\mu(\mathbf{r})$ are determined by self-consistently solving modified Kohn-Sham equations for an isolated confined atom using DFT [5]:

$$\left[\hat{T}_s + V_i^{\mathrm{eff}}[n](\mathbf{r})\right] \varphi_\mu(\mathbf{r}) = \epsilon_\mu^{\mathrm{eff}} \varphi_\mu(\mathbf{r}), \quad \forall \mu \tag{6}$$

where the effective potential $V_i^{\mathrm{eff}}[n](\mathbf{r})$

$$V_i^{\mathrm{eff}}[n](\mathbf{r}) = V_{\mathrm{ext},i}(\mathbf{r}) + V_{\mathrm{H}}[n](\mathbf{r}) + V_{\mathrm{xc}}^{LDA}[n](\mathbf{r}) + \left(\frac{r_i}{r_0}\right)^N, \tag{7}$$

additionally contains a confining potential introduced to improve performance [7]. $V_{\mathrm{ext},i}(\mathbf{r})$ is the electrostatic potential from the ion i, and $r_i = |\mathbf{r}_i| = |\mathbf{r} - \mathbf{R}_i|$.

Following Ref.[1], the Hamiltonian matrix elements $H_{\mu\nu}^0$ are evaluated using the two-centre approximation

$$H_{\mu\nu}^0 = \begin{cases} \epsilon_\mu^{\mathrm{atom}} & \mu = \nu \\ \langle \varphi_\mu | \hat{T}_s + V_i + V_j | \varphi_\nu \rangle & i \neq j \\ 0 & i = j, \mu \neq \nu. \end{cases} \tag{8}$$

V_i is the effective free atom potential of atom i given by the expression in Eq. 7 but without the confining potential. The diagonal term $\epsilon_\mu^{\mathrm{atom}}$ is the energy eigenvalue obtained by solving Eq. 6 again omitting the confining potential.

Regarding the second order energy in Eq. 2, if the local density approximation

(LDA) is used for exchange-correlation contributions, then these vanish when $\mathbf{r} \neq \mathbf{r}'$. Ignoring the on-site term of the exchange-correlation contributions, then only the electrostatic interaction from charge fluctuations remain. The fluctuation $\delta n(\mathbf{r})$ can be partitioned into atom-centred contributions $\delta n(\mathbf{r}) = \sum_i \delta n_i(\mathbf{r}_i)$, each expressed as a superposition of multipole densities $\delta n_i(\mathbf{r}) = \sum_\ell \rho_i(\mathbf{r})[\Delta Q_\ell]$, where ℓ is the number denoting the rank of the Cartesian multipole [1]. The multipole densities themselves $\rho_i(\mathbf{r})[\Delta Q_\ell]$ can be expressed in terms of a standard normalised isotropic density $\rho_i^{\text{iso}}(r)$ scaled by the multipole moment ΔQ_ℓ. For example, dipole densities can be constructed from $\rho_i^{\text{iso}}(r)$ in an analogous manner to how a standard dipole can be constructed from opposing point charges.

Standard SCC-DFTB uses the monopole approximation, in which the expansion of the density fluctuation only includes the charge difference

$$\delta n_i(\mathbf{r}) \approx \rho_i(\mathbf{r})[\Delta q_i] = \Delta q_i \rho_i^{\text{iso}}(r). \tag{9}$$

Then $E_{2\text{nd}}$ becomes

$$E_{2\text{nd}} = \frac{1}{2}\sum_{i=1}^{N}\sum_{j=1}^{N}\int\int \frac{\delta n_i(\mathbf{r}_i)\delta n_j(\mathbf{r}'_j)}{|\mathbf{r}-\mathbf{r}'|} d\mathbf{r}d\mathbf{r}' = \frac{1}{2}\sum_{i=1}^{N}\sum_{j=1}^{N}\Delta q_i \hat{\Gamma}_{ij}^{00}\Delta q_j \tag{10}$$

where

$$\hat{\Gamma}_{ij}^{00} = \int\int \frac{\rho_i^{\text{iso}}(r_i)\rho_j^{\text{iso}}(r'_j)}{|\mathbf{r}-\mathbf{r}'|} d\mathbf{r}d\mathbf{r}'. \tag{11}$$

Analytical forms such as those based upon normalised Gaussian or exponential-decay distributions $\rho_{i,\text{GAU}}^{\text{iso}}(r) = (\sigma_i/\pi)^{3/2} e^{-\sigma_i r^2}$ and $\rho_{i,\text{EXP}}^{\text{iso}}(r) = \left(\tau_i^3/8\pi\right) e^{-\tau_i r}$ respectively, are adopted for $\rho^{\text{iso}}(r)$ to evaluate $\hat{\Gamma}_{ij}^{00}$, introducing a parameter (σ_i or τ_i) for

[1] For example, Q_1 denotes the dipole moment made from p_x, p_y and p_z components.

each atom. Then

$$\hat{\Gamma}^{00}_{ij,\mathrm{GAU}} = \begin{cases} \frac{1}{R_{ij}}\,\mathrm{erf}\left(\sqrt{\frac{\sigma_i\sigma_j}{\sigma_i+\sigma_j}}R_{ij}\right) & i \neq j \\ \sqrt{\frac{2\sigma_i}{\pi}} & i = j, \end{cases}$$

$$\hat{\Gamma}^{00}_{ij,\mathrm{EXP}} = \begin{cases} \frac{1}{R_{ij}} - e^{-\tau_i R_{ij}}\left(\frac{\tau_j^4\tau_i}{2(\tau_i^2-\tau_j^2)^2} - \frac{\tau_j^6-3\tau_j^4\tau_i^2}{(\tau_i^2-\tau_j^2)^3 R_{ij}}\right) & \\ -e^{-\tau_j R_{ij}}\left(\frac{\tau_i^4\tau_j}{2(\tau_j^2-\tau_i^2)^2} - \frac{\tau_i^6-3\tau_i^4\tau_j^2}{(\tau_j^2-\tau_i^2)^3 R_{ij}}\right) & i \neq j, \tau_i \neq \tau_j \\ \frac{1}{R_{ij}} - e^{-\tau_i R_{ij}}\left(\frac{1}{R_{ij}} + \frac{11}{16}\tau_i + \frac{3}{16}\tau_i^2 R_{ij} + \frac{1}{48}\tau_i^3 R_{ij}^2\right) & i \neq j, \tau_i = \tau_j \\ \frac{5}{16}\tau_i & i = j, \end{cases} \tag{12}$$

where $R_{ij} = |\mathbf{R}_i - \mathbf{R}_j|$. The on-site value $\hat{\Gamma}^{00}_{ii}$ is directly related to σ_i (τ_i), meaning the parameter can be obtained from $\hat{\Gamma}^{00}_{ii}$ which can be approximated by the difference of ionization energy I_i and electron affinity A_i of the atom, or the Hubbard U [3] : $\hat{\Gamma}^{00}_{ii} = U_i \approx I_i - A_i$.

$$\hat{\Gamma}^{00}_{ii,\mathrm{GAU}} = \sqrt{\frac{2\sigma_i}{\pi}} = U_i \quad \Rightarrow \quad \sigma_i = \frac{\pi}{2}U_i^2. \tag{13}$$

$$\hat{\Gamma}^{00}_{ii,\mathrm{EXP}} = \frac{5}{16}\tau_i = U_i \quad \Rightarrow \quad \tau_i = \frac{16}{5}U_i. \tag{14}$$

The charge difference Δq_i, itself, is calculated as $\Delta q_i = q_i - q_i^0$, with q_i^0 the valence charge of the reference atom. Mulliken population analysis [8] is used in SCC-DFTB scheme [2] to determine charge q_i as

$$q_i = e\frac{1}{2}\sum_k f_k \sum_\alpha \sum_\nu \left(c_\mu^{k*} c_\nu^k S_{\mu\nu} + c_\nu^{k*} c_\mu^k S_{\mu\nu}^*\right), \tag{15}$$

with $S_{\mu\nu}$ the orbital overlap

$$S_{\mu\nu} = \int \varphi_\mu^*(\mathbf{r})\varphi_\nu(\mathbf{r})\,d\mathbf{r}. \tag{16}$$

Eigenvector coefficients c_μ^k are obtained by minimising the total energy subject to

fixed particle number. This yields a set of Kohn-Sham like equations,

$$\sum_{\nu}\left(H^0_{\mu\nu}+H^1_{\mu\nu}-\epsilon_k S_{\mu\nu}\right)c^k_\nu=0, \tag{17}$$

where the Hamiltonian elements shift $H^1_{\mu\nu}$ is introduced, and here defined as

$$H^1_{\mu\nu}=e\frac{1}{2}\sum_{h=1}^{N}\left(S_{\mu\nu}\hat{\Gamma}^{00}_{ih}+S^*_{\nu\mu}\hat{\Gamma}^{00}_{jh}\right)\Delta q_h. \tag{18}$$

3. Dipole approximation

The monopole approximation used in SCC-DFTB has fundamentally improved the accuracy of the DFTB allowing for the incorporation of charge transfer effects. However, for highly polarised systems extending the approximation is desirable. At the next level of approximation the atomic charge density fluctuation $\delta n_i(\mathbf{r})$ can be expressed as a superposition of a density $\rho_i(\mathbf{r})[\Delta q_i]$ associated with charge difference Δq_i, and a density $\rho_i(\mathbf{r})[\Delta\mathbf{p}_i]$ associated with dipole difference $\Delta\mathbf{p}_i$:

$$\delta n_i(\mathbf{r})=\rho_i(\mathbf{r})[\Delta q_i]+\tilde{\rho}_i(\mathbf{r})[\Delta\mathbf{p}_i]. \tag{19}$$

The charge part has been considered above. For the terms containing the influence of the dipole part of the density, we can consider this as resulting from two opposite signed charge densities displaced from atom center $\mathbf{R}_i$ by $\pm d$ ($\lim_{d\to 0}$) in the direction of dipole $\Delta\mathbf{p}_i$. These charge densities are taken to have distribution $\tilde{\rho}^{\mathrm{iso}}_i(r)$, and magnitude $|\Delta\mathbf{p}_i|/d$:

$$\tilde{\rho}_i(\mathbf{r})[\Delta\mathbf{p}_i]=\Delta\mathbf{p}_i\cdot\nabla_{\mathbf{R}_i}\tilde{\rho}^{\mathrm{iso}}_i(r_i) \tag{20}$$

where $\nabla_{\mathbf{R}_i}$ denotes that ∇ operates which respect to the atomic center $\mathbf{R}_i$. Note that $\tilde{\rho}^{\mathrm{iso}}_i(r)$ used to describe the dipole fluctuation density need not be the same as $\rho^{\mathrm{iso}}_i(r)$ which describes the charge fluctuation density. Still using Gaussian or exponential-decay forms for $\tilde{\rho}_i$, this will lead to one more free parameter.

The second order energy is now

$$
\begin{aligned}
E_{\mathrm{2nd}} = & \frac{1}{2}\sum_{i=1}^{N}\sum_{j=1}^{N}\int\int \frac{\delta n_i(\mathbf{r}_i)\delta n_j(\mathbf{r}'_j)}{|\mathbf{r}-\mathbf{r}'|}d\mathbf{r}d\mathbf{r}' = \frac{1}{2}\sum_{i=1}^{N}\sum_{j=1}^{N}\Delta q_i \hat{\Gamma}^{00}_{ij}\Delta q_j \\
& + \sum_{i=1}^{N}\sum_{j=1}^{N}\Delta\mathbf{p}_i\cdot\left(\nabla_{\mathbf{R}_i}\int\int \frac{\tilde{\rho}^{\mathrm{iso}}_i(r_i)\rho^{\mathrm{iso}}_j(r'_j)}{|\mathbf{r}-\mathbf{r}'|}d\mathbf{r}d\mathbf{r}'\right)\Delta q_j \\
& + \frac{1}{2}\sum_{i=1}^{N}\sum_{j=1}^{N}\Delta\mathbf{p}_i\cdot\left(\nabla_{\mathbf{R}_j}\otimes\nabla_{\mathbf{R}_i}\int\int \frac{\tilde{\rho}^{\mathrm{iso}}_i(r_i)\tilde{\rho}^{\mathrm{iso}}_j(r'_j)}{|\mathbf{r}-\mathbf{r}'|}d\mathbf{r}d\mathbf{r}'\right)\Delta\mathbf{p}_j.
\end{aligned}
\tag{21}
$$

Similar to $\hat{\Gamma}^{00}_{ij}$ (scalar), we introduce $\hat{\Gamma}^{10}_{ij}$ (vector) and $\hat{\Gamma}^{11}_{ij}$ (tensor) as

$$
\hat{\Gamma}^{10}_{ij} = \nabla_{\mathbf{R}_i}\int\int \frac{\tilde{\rho}^{\mathrm{iso}}_i(r_i)\rho^{\mathrm{iso}}_j(r'_j)}{|\mathbf{r}-\mathbf{r}'|}d\mathbf{r}d\mathbf{r}', \tag{22}
$$

$$
\hat{\Gamma}^{11}_{ij} = \nabla_{\mathbf{R}_j}\otimes\nabla_{\mathbf{R}_i}\int\int \frac{\tilde{\rho}^{\mathrm{iso}}_i(r_i)\tilde{\rho}^{\mathrm{iso}}_j(r'_j)}{|\mathbf{r}-\mathbf{r}'|}d\mathbf{r}d\mathbf{r}', \tag{23}
$$

so that

$$
E_{\mathrm{2nd}} = \frac{1}{2}\sum_{i=1}^{N}\sum_{j=1}^{N}\Delta q_i\hat{\Gamma}^{00}_{ij}\Delta q_j + \sum_{i=1}^{N}\sum_{j=1}^{N}\Delta\mathbf{p}_i\cdot\hat{\mathbf{\Gamma}}^{10}_{ij}\Delta q_j + \frac{1}{2}\sum_{i=1}^{N}\sum_{j=1}^{N}\Delta\mathbf{p}_i\cdot\hat{\mathbf{\Gamma}}^{11}_{ij}\Delta\mathbf{p}_j, \tag{24}
$$

representing charge-charge (qq), charge-dipole (pq) and dipole-dipole (pp) contributions. Expressions for $\hat{\mathbf{\Gamma}}^{10}_{ij}$ and $\hat{\mathbf{\Gamma}}^{11}_{ij}$ can be obtained similarly to $\hat{\Gamma}^{00}_{ij}$ (see Appendix A), with the specific form dependent upon the choice of isotropic distributions.

As with Δq_i, the dipole difference $\Delta\mathbf{p}_i$ can also be obtained by Mulliken population analysis. The total dipole of the system is

$$
\mathbf{p} = \int \mathbf{r}\rho(\mathbf{r})d\mathbf{r} = e\sum_k f_k\sum_\mu\sum_\nu c^{k*}_\mu c^k_\nu\left[\mathbf{R}_i\int\varphi^*_\mu(\mathbf{r})\varphi_\nu(\mathbf{r})d\mathbf{r} + \int\mathbf{r}_i\varphi^*_\mu(\mathbf{r})\varphi_\nu(\mathbf{r})d\mathbf{r}\right]. \tag{25}
$$

Introducing dipole matrix elements $\mathbf{P}_{\mu\nu}$ as

$$
\mathbf{P}_{\mu\nu} = \int\mathbf{r}_i\varphi^*_\mu(\mathbf{r})\varphi_\nu(\mathbf{r})d\mathbf{r} \tag{26}
$$

where the integral is over all space, then

$$\mathbf{p} = e\sum_k f_k \sum_\mu \sum_\nu c_\mu^{k*} c_\nu^k \mathbf{R}_i S_{\mu\nu} + e\sum_k f_k \sum_\mu \sum_\nu c_\mu^{k*} c_\nu^k \mathbf{P}_{\mu\nu}. \tag{27}$$

The total dipole moment of the system is seen to be made up of two contributions, the first the macroscopic part $\mathbf{p}_{\text{ext}}$ due to charges distributed on atoms throughout the system, and the second the atomic part $\mathbf{p}_{\text{int}}$ due to the atomic dipole distributions. Similar to the way Mulliken charges are defined in Eq. 15, the dipole contribution can be decomposed into a sum over atomic contributions by defining

$$\begin{aligned}
\mathbf{p}_{\text{ext}}^i &= \mathbf{R}_i e\frac{1}{2}\sum_k f_k \sum_\alpha \sum_\nu \left(c_\mu^{k*} c_\nu^k S_{\mu\nu} + c_\nu^{k*} c_\mu^k S_{\mu\nu}^*\right) = \mathbf{R}_i q_i \\
\mathbf{p}_{\text{int}}^i &= e\frac{1}{2}\sum_k f_k \sum_\alpha \sum_\nu \left(c_\mu^{k*} c_\nu^k \mathbf{P}_{\mu\nu} + c_\nu^{k*} c_\mu^k \mathbf{P}_{\mu\nu}^*\right),
\end{aligned} \tag{28}$$

so that $\mathbf{p} = \sum_i \left(\mathbf{p}_{\text{ext}}^i + \mathbf{p}_{\text{int}}^i\right)$, where $\mathbf{p}_{\text{ext}}^i$ is the atomic contribution associated with the net charge on atom. Because the initial reference dipole of the free atom is zero, we can identify the atomic contribution from dipole distributions on each atom $\mathbf{p}_{\text{int}}^i$ as the dipole difference on each atom, which is therefore to be used in Eq. 24.

In order to find $\mathbf{P}_{\mu\nu}$ in Eq. 26, it is convenient to define artificial orbitals $\chi_\mu^\xi(\mathbf{r})$

$$\chi_\mu^\xi(\mathbf{r}) = \hat{\mathbf{e}}_\xi \cdot \left(\mathbf{r}_i \varphi_\mu(\mathbf{r})\right) \qquad \xi = x, y, z \tag{29}$$

so that

$$\mathbf{r}_i \varphi_\mu(\mathbf{r}) = \sum_\xi \hat{\mathbf{e}}_\xi \chi_\mu^\xi(\mathbf{r}). \tag{30}$$

Since we can write $\mathbf{r} = \sum_\xi \hat{\mathbf{e}}_\xi r\sqrt{4\pi/3}Y_\xi(\theta,\phi)$, where Y_ξ is a spherical harmonic, then

$$\begin{aligned}
\mathbf{r}_i \varphi_\mu(\mathbf{r}) &= \sum_\xi \hat{\mathbf{e}}_\xi \left(r_i\sqrt{\frac{4\pi}{3}}Y_\xi(\theta_i,\phi_i)\right)\left(R_\mu(r_i)Y_\alpha(\theta_i,\phi_i)\right) \\
&= \sum_\xi \hat{\mathbf{e}}_\xi \left(r_i R_\mu(r_i)\right)\sum_\omega C_{\alpha,\xi}^\omega Y_\omega(\theta_i,\phi_i),
\end{aligned} \tag{31}$$

allowing the identification of

$$\chi_{\mu}^{\xi}(\mathbf{r}) = r_i R_{\mu}(r_i) \sum_{\omega} C_{\alpha,\xi}^{\omega} Y_{\omega}(\theta_i, \phi_i). \tag{32}$$

where the coefficients $C_{\alpha,\xi}^{\omega}$ are given by integral over the spherical surface

$$C_{\alpha,\xi}^{\omega} = \sqrt{\frac{4\pi}{3}} \int Y_{\omega}(\theta,\phi) Y_{\alpha}(\theta,\phi) Y_{\xi}(\theta,\phi) \sin\theta d\theta d\phi. \tag{33}$$

In this way, Eq. 26 becomes

$$\mathbf{P}_{\mu\nu} = \int \mathbf{r}_i \varphi_{\mu}^{*}(\mathbf{r}) \varphi_{\nu}(\mathbf{r}) d\mathbf{r} = \sum_{\xi} \hat{\mathbf{e}}_{\xi} \int \chi_{\mu}^{\xi *}(\mathbf{r}) \varphi_{\nu}(\mathbf{r}) d\mathbf{r}, \tag{34}$$

which have same form as the $S_{\mu\nu}$, so similar techniques can be used to evaluate $\mathbf{P}_{\mu\nu}$ numerically for each atom pair.

Finally, the same method as used to obtain Eq. 18 gives the Hamiltonian shift including dipole fluctuation as

$$\begin{aligned} H_{\mu\nu}^{1} = & e\frac{1}{2}\sum_{h=1}^{N} [\ (S_{\mu\nu}\hat{\Gamma}_{ih}^{00} + S_{\nu\mu}^{*}\hat{\Gamma}_{jh}^{00})\Delta q_h \\ & + (\mathbf{P}_{\mu\nu}\cdot\hat{\mathbf{\Gamma}}_{ih}^{10} + \mathbf{P}_{\nu\mu}^{*}\cdot\hat{\mathbf{\Gamma}}_{jh}^{10})\Delta q_h + \Delta\mathbf{p}_h\cdot(\hat{\mathbf{\Gamma}}_{hi}^{10}S_{\mu\nu} + \hat{\mathbf{\Gamma}}_{hj}^{10}S_{\nu\mu}^{*}) \\ & + (\mathbf{P}_{\mu\nu}\cdot\hat{\mathbf{\Gamma}}_{ih}^{11} + \mathbf{P}_{\nu\mu}^{*}\cdot\hat{\mathbf{\Gamma}}_{jh}^{11})\Delta\mathbf{p}_h\ ]. \end{aligned} \tag{35}$$

When an external electric field is present, the energy due to interaction with this field produces an additional contribution to the second order energy as

$$E_{2\mathrm{nd}} = E_{2\mathrm{nd}}^{\mathrm{qq}} + E_{2\mathrm{nd}}^{\mathrm{pq}} + E_{2\mathrm{nd}}^{\mathrm{pp}} + \sum_{i=1}^{N}\Delta q_i V_i^{\mathrm{ext}} - \sum_{i=1}^{N}\Delta\mathbf{p}_i\cdot\mathbf{E}_i^{\mathrm{ext}}. \tag{36}$$

where $\mathbf{E}_i^{\mathrm{ext}}$ is the external field at the location of atom i, and V_i^{ext} the corresponding external potential. This then results in an additional contribution $H_{\mu\nu}^{\mathrm{ext}}$ to be added to the Hamiltonian shift in Eq. 35, namely

$$H_{\mu\nu}^{\mathrm{ext}} = e\frac{1}{2}\left[(S_{\mu\nu}V_i^{\mathrm{ext}} + S_{\nu\mu}^{*}V_j^{\mathrm{ext}}) - (\mathbf{P}_{\mu\nu}\cdot\mathbf{E}_i^{\mathrm{ext}} + \mathbf{P}_{\nu\mu}^{*}\cdot\mathbf{E}_j^{\mathrm{ext}})\right]. \tag{37}$$

and the total Hamiltonian matrix becomes

$$H_{\mu\nu} = H^0_{\mu\nu} + H^1_{\mu\nu} + H^{\text{ext}}_{\mu\nu}. \tag{38}$$

The above equation represents our self-consistent charge and dipole DFTB scheme (SCCD-DFTB).

4. Applications to Carbon Based Systems

An implementation of the above SCCD-DFTB scheme has been made, based upon the existing SCC-DFTB code "DFTB+" [3; 9]. The Slater-Koster integrals for the dipole matrix $\mathbf{P}_{\mu\nu}$ have been generated separately based on the 'pbc-0-1' parametrization, and calculation of $\hat{\mathbf{\Gamma}}^{10}_{ij}/\hat{\mathbf{\Gamma}}^{11}_{ij}$, Mulliken dipole difference $\Delta\mathbf{p}_i$ and inclusion of an external field $\mathbf{E}^{\text{ext}}_i$ are implemented along with the necessary modifications to the total energy and Hamiltonian shift.

We describe both the charge and dipole distribution using the same analytical forms, for which we use the exponential-decay profile $\rho^{\text{iso}}(r) = \left(\tau^3/8\pi\right) e^{-\tau r}$, but note that the parameter τ that enters need not be the same where describing both charge and dipole distributions. We use calculations performed on different fullerene molecules (C60, C70 and C84) and carbon nanotubes (CNT) ((6,6), (9,0) and (15,0)) to explore this parametrisation. All systems are treated as non-periodic clusters, with lengths greater than 40 Å used for the CNTs to ensure that edge effects are negligible. The geometries of the fullerenes are those obtained by relaxing atomic coordinates using SCC-DFTB, and the geometries of the CNTs are those used in Ref. [10]. Polarizabilities for each system have been calculated as the value of the parameter τ for the dipole distribution (τ_p) is varied, while holding that for the charge (τ_q) fixed. The standard value for charge parameter $\tau_q = 1.16$ obtained using Eq. 14 is used. The polarizability α is acquired using the relation $\mathbf{P} = \alpha\mathbf{E}$, where $\mathbf{E}$ is the applied electric field and $\mathbf{P}$ the resulting static dipole, and we present results for the mean polarizability for fullerenes or lateral polarizability per unit length ($\alpha_\perp$) for CNTs. Note that the dipole $\mathbf{P}$ here is the total dipole of the system, a combination of the atomic

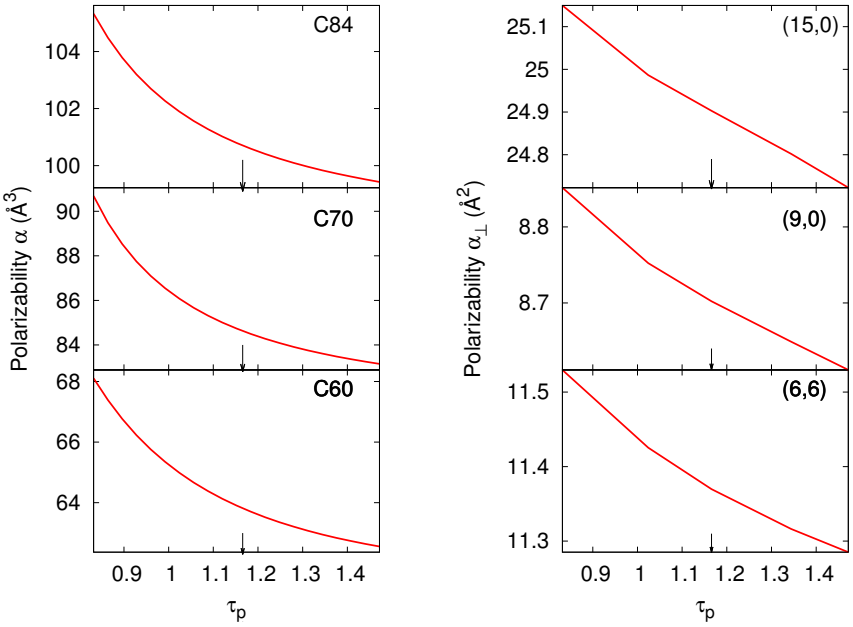

Figure 1: Calculated mean polarizability of various fullerenes and lateral polarizability per unit length of various CNTs using SCCD-DFTB with different parameter value τ_p for dipole distribution. The arrows indicate the standard parameter for charge τ_q.

dipole on each atom and the dipole due to the distribution of the charges. We observe a sudden band gap closing and total energy jump for fullerenes when τ_p is too small (0.64, 0.672, 0.768 for C60, C70, C84), indicating that τ_p smaller than those values is not physical. Instead we limit the range of value τ_p to within ± 30% of the standard charge parameter, so between 0.832 and 1.472. Fig. 1 shows that all systems exhibit similar trends: smaller τ_p results in larger polarizability. The set of fullerenes (left panel in Fig. 1) and the set of CNTs (right panel in Fig. 1) also show similar variations.

Table 1 gives the polarizabilities of selected fullerenes and CNTs calculated from SCC-DFTB and two sets of results from SCCD-DFTB using for the dipole parameter either $\tau_p = \tau_q$ or $\tau_p = 0.832$, along with other experimental and theoretical results from references [10–13; 16–18]. Results obtained using $\tau_p = 0.832$ are presented as this value of the parameter yields the maximum polarizabilities for all systems with τ_p in the range considered. With $\tau_p = \tau_q$, the results obtained using SCCD-DFTB

Table 1: Calculated polarizabilities (α or $\alpha_\perp$) of various carbon-based systems using self-consistent charge (SCC) and dipole extension (SCCD) DFTB with different parameters τ_p, compared with previous calculated and experimental results.

		C60	C70	C84
(Å^3)	SCC-DFTB	58.0	77.7	93.2
	SCCD-DFTB ($\tau_p = \tau_q$)	63.9	84.6	100.7
	SCCD-DFTB ($\tau_p = 0.832$)	68.1	90.6	105.3
	MCSCF[a]	75.1	89.8	109.4
	charge-dipole[b]	75.1	91.5	115.9
	DFT-LDA[c]	86.1	104.8	
	DFT-PBE[d]	82.9	102.8	
	exp [f]	83.0	103.5	
	exp [g]	76.5±8		
	exp[h]			102±14

		CNT(6,6)	CNT(9,0)	CNT(15,0)
(Å^2)	SCC-DFTB	10.7	8.0	23.1
	SCCD-DFTB ($\tau_p = \tau_q$)	11.4	8.7	24.9
	SCCD-DFTB ($\tau_p = 0.832$)	11.5	8.9	25.2
	MCSCF[a]	11.0	8.9	20.1
	charge-dipole[b]	11.3	8.9	21.5
	DFT-PBE[e]	11.6	9.3	20.3

[a] Multi-Configurational Self-Consistent Field [11]
[b] Classical charge-dipole [10]
[c] DFT-LDA [12]
[d] DFT-PBE [13]
[e] DFT-PBE [14]
[e] Experimental method (electron energy loss spectroscopy) [15]
[f] Experimental method (molecular beam deflection) [16]
[g] Experimental method (gas phase) [17]

show a ~ 9% enhancement in polarizabilities over charge only SCC-DFTB for both fullerenes and CNTs, while with $\tau_p = 0.832$, the polarizabilities are enhanced over the SCC-DFTB value by ~ 16 % for fullerenes and ~ 9% for CNTs. Further analysis of the parameter sensitivity of the two sets of systems (see Appendix B) shows that the observed differences are mainly due to the different nature of their polarizability, namely that polarizability of the fullerenes is the mean value for the molecule (Å^3) and that of CNTs is the lateral polarizability per unit length (Å^2).

The above results for a set of 3 CNTs shows little enhancement in the calculated polarizabilities when using $\tau_p = 0.832$, which gives the maximum calculated polar-

izabilities, when compared to those obtained using $\tau_p = \tau_q$. Additional calculations on 12 CNTs ((3,3), (4,4), (5,5), (6,6), (7,0), (8,0), (9,0), (10,0), (11,0), (6,2), (6,4) and (8,4)) with the dipole charge distribution parameter $\tau_p = \tau_q$ and $\tau_p = 0.832$ have also been performed, and give average lateral polarizability enhancements of 9.3 % and 10.2 % respectively over charge only SCC-DFTB results, confirming that CNT systems are not particularly sensitive to the parameter τ_p.

As Refs. [19–24] have suggested, the lateral polarizability of CNTs shows a linear dependence on the square of their radius. Fig. 2 shows a comparison of calculated polarizabilities of these 12 CNT systems presented so as to show this, and as obtained from SCC-DFTB, SCCD-DFTB using $\tau_p = \tau_q$, and DFT results using the PBE functional reported in Ref. [14]. DFT-PBE results are chosen for comparison because Table 1 shows that among other simulation methods, DFT calculation results and experimental measurements agree best and because the set of DFTB parameters used in this paper have been derived by fitting to the results of DFT calculations that used the PBE functional. Fig. 2 shows that there is a systematic enhancement of the polarizabilities moving from SCC-DFTB to SCCD-DFTB, the latter mostly showing a $8 \sim 12\%$ improvement comparing to DFT-PBE values.

Although the above results on fullerenes and CNTs indicate that the SCCD-DFTB method shows systematic improvement over SCC-DFTB, there still remain difference with values derived from experiment or calculations using ab-initio DFT methods. In this regard, firstly, differences between some calculated values may reflect slight differences in geometries used, with a 0.04 Å variation in bond length in fullerenes and CNTs changing polarizabilities by $\sim 4\%$. Secondly, we note that the basis sets used in standard DFTB are minimal basis sets, restricting the variational freedom to describe charge redistribution. Taking monolayer graphene as an example, we find a perpendicular static dipole moment of $\simeq 0.3$ Å^3 per unit cell using SCCD-DFTB with a minimal basis set, the precise value depending upon the parameterisation. This is a significant improvement over the vanishing value found with standard charge-only SCC-DFTB, but below ab-initio DFT values (see Appendix C), and consistent with the trend that sees $\alpha_\perp$ increase with basis set size. While preparing this manuscript, Boleininger et al. [25] have reported a study using DFTB that

shows that both an increased basis set along with dipole corrections improves the description of the polarizabilities of hydrocarbon molecules. Their approach incorporates self-consistent polarized charges and polarization orbitals, with multipole interactions calculated "on-the-fly", reported as contributing a notable computational overhead. This is avoided in the approach adopted here. We also note that whereas the approach considered here considers multipole contributions as a coupled self-consistent charge process, alternative methods have been proposed to address polarization within the DFTB framework that considering dipole interactions independently of the self-consistent charge, such as the chemical potential equalization method [26–28] and SCC-DFTB with force field method [29]. Finally, both SCC- and this SCCD-DFTB extension are based upon the second-order approximation, with higher order terms in the density fluctuation expansion of the total energy ignored, while Gaus et al. [30] have argued that third-order terms are particularly important for the description of systems with localized charges. Nevertheless, when future improvements in basis set, higher-order corrections and other possible improvement have been made, the dipole extension discussed here can be easily adapted accordingly, providing further accuracy with little extra cost.

5. Conclusion

In conclusion, we have extended the standard SCC-DFTB method from monopole to dipole approximation. Implementing the extension within the "DFTB+" code, we have applied it to various carbon systems and discussed the parametrization of the dipole extension. Comparing with ab-initio DFT calculations, we find calculated polarizabilities of a set of 12 CNTs, are improved using our SCCD-DFTB scheme over those obtained from charge only SCC-DFTB. We expect more generally that SCCD-DFTB method increases accuracy for systems with significant charge asymmetry, while preserving the low cost of the computational approach.

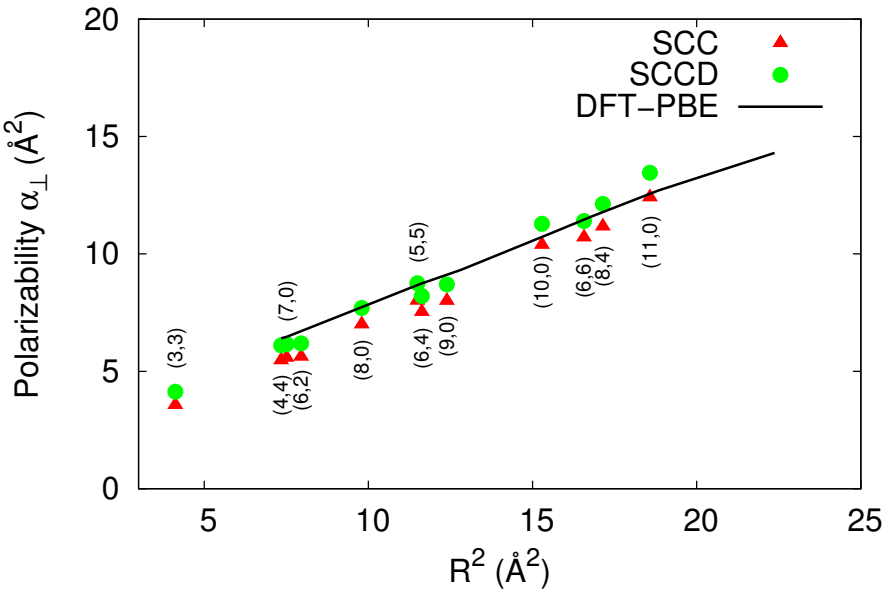

Figure 2: Calculated lateral polarizability with respect to radius squared of a set of CNTs using SCC- and SCCD-DFTB, and for comparison results using DFT-PBE from Ref. [14].

Acknowledgement

This work was supported by a Science and Innovation Award (EP/G036101/1) from the United Kingdom Engineering and Physical Sciences Research Council. YW gratefully acknowledges a University Research Studentship from the University of Bath.

Appendix A. Charge-charge, charge-dipole and dipole-dipole interaction matrices.

$\hat{\mathbf{\Gamma}}^{10}_{ij}$. As defined in Eq. 22

$$\hat{\mathbf{\Gamma}}^{10}_{ij} = \nabla_{\mathbf{R}_i} \int\int \frac{\rho^{\mathrm{iso}}_i(r_i)\rho^{\mathrm{iso}}_j(r_j)}{|\mathbf{r}-\mathbf{r}'|} d\mathbf{r}d\mathbf{r}' = \nabla_{\mathbf{R}_i}\hat{\Gamma}^{00}_{ij}. \tag{A.1}$$

For the Gaussian distribution, this gives immediately

$$\hat{\mathbf{\Gamma}}^{10}_{ij,\mathrm{GAU}} = \frac{\mathbf{R}_{ij}}{R^3_{ij}}\left[-\mathrm{erf}\left(\sqrt{\frac{\sigma_i\sigma_j}{\sigma_i+\sigma_j}}R_{ij}\right)+\sqrt{\frac{4\sigma_i\sigma_j}{\pi(\sigma_i+\sigma_j)}}R_{ij}e^{-\frac{\sigma_i\sigma_j}{\sigma_i+\sigma_j}R^2_{ij}}\right], \tag{A.2}$$

while for the exponential-decay distribution, the result is

$$\hat{\mathbf{\Gamma}}^{10}_{ij,\mathrm{EXP}} = -\frac{\mathbf{R}_{ij}}{R^3_{ij}} - \mathbf{R}_{ij}\begin{cases} e^{-\tau_i R_{ij}}\left(-\frac{\tau_j^4\tau_i}{2(\tau_i^2-\tau_j^2)^2}\frac{\tau_i}{R_{ij}}+\frac{\tau_j^6-3\tau_j^4\tau_i^2}{(\tau_i^2-\tau_j^2)^3}\frac{\tau_i}{R^2_{ij}}+\frac{\tau_j^6-3\tau_j^4\tau_i^2}{(\tau_i^2-\tau_j^2)^3}\frac{1}{R^3_{ij}}\right) & \\ +e^{-\tau_j R_{ij}}\left(-\frac{\tau_i^4\tau_j}{2(\tau_j^2-\tau_i^2)^2}\frac{\tau_j}{R_{ij}}+\frac{\tau_i^6-3\tau_i^4\tau_j^2}{(\tau_j^2-\tau_i^2)^3}\frac{\tau_j}{R^2_{ij}}+\frac{\tau_i^6-3\tau_i^4\tau_j^2}{(\tau_j^2-\tau_i^2)^3}\frac{1}{R^3_{ij}}\right) & i\neq j, \tau_i\neq\tau_j \\ -e^{-\tau_i R_{ij}}\left(\frac{1}{R^3_{ij}}+\frac{\tau_i}{R^2_{ij}}+\frac{\tau_i^2}{2R_{ij}}+\frac{7\tau_i^3}{48}+\frac{\tau_i^4 R_{ij}}{48}\right) & i\neq j, \tau_i=\tau_j \end{cases} \tag{A.3}$$

Because of symmetry, the on-site values for $\hat{\mathbf{\Gamma}}^{10}_{ii,\mathrm{GAU}}$ and $\hat{\mathbf{\Gamma}}^{10}_{ii,\mathrm{EXP}}$ are both $\mathbf{0}$.

$\hat{\mathbf{\Gamma}}^{11}_{ij}$. As defined in Eq. 23

$$\begin{aligned}\hat{\mathbf{\Gamma}}^{11}_{ij} &= \nabla_{\mathbf{R}_j}\otimes\nabla_{\mathbf{R}_i}\int\int\frac{\rho_i^{\mathrm{iso}}(r_i)\rho_j^{\mathrm{iso}}(r_j)}{|\mathbf{r}-\mathbf{r}'|}d\mathbf{r}d\mathbf{r}' \\ &= \nabla_{\mathbf{R}_j}\otimes\nabla_{\mathbf{R}_i}\hat{\Gamma}^{00}_{ij} \\ &= \nabla_{\mathbf{R}_j}\otimes\hat{\mathbf{\Gamma}}^{10}_{ij} = -\nabla_{\mathbf{R}_i}\otimes\hat{\mathbf{\Gamma}}^{10}_{ij}.\end{aligned} \tag{A.4}$$

In this case, $\nabla_{\mathbf{R}_i}$ is differentiation with respect to the same vector as in $\hat{\mathbf{\Gamma}}^{10}_{ij}$.

For both Gaussian distribution and exponential-decay distribution cases, $\hat{\mathbf{\Gamma}}^{10}_{ij}$ has the form $\hat{\mathbf{\Gamma}}^{10}_{ij} = \mathbf{R}_{ij}F(\mathbf{R}_{ij})$. For vector $\mathbf{a} = \mathbf{r}F(r)$,

$$\nabla\otimes\mathbf{a} = F\mathbf{I} + \frac{1}{r}\frac{\partial F}{\partial r}\mathbf{r}\otimes\mathbf{r}, \tag{A.5}$$

where $\mathbf{I}$ is the 3×3 identity matrix. Therefore, for the Gaussian distribution becomes

$$\begin{aligned}\hat{\mathbf{\Gamma}}^{11}_{ij,\mathrm{GAU}} = &\frac{3\mathbf{R}_{ij}\otimes\mathbf{R}_{ij}-R^2_{ij}\mathbf{I}}{R^5_{ij}}\left[-\mathrm{erf}\left(\sqrt{\frac{\sigma_i\sigma_j}{\sigma_i+\sigma_j}}R_{ij}\right)+\sqrt{\frac{4\sigma_i\sigma_j}{\pi(\sigma_i+\sigma_j)}}R_{ij}e^{-\frac{\sigma_i\sigma_j}{\sigma_i+\sigma_j}R^2_{ij}}\right] \\ &+\frac{1}{R^2_{ij}}\sqrt{\frac{16\sigma_i^3\sigma_j^3}{\pi(\sigma_i+\sigma_j)^3}}e^{-\frac{\sigma_i\sigma_j}{\sigma_i+\sigma_j}R^2_{ij}}\mathbf{R}_{ij}\otimes\mathbf{R}_{ij}.\end{aligned} \tag{A.6}$$

The on-site $\hat{\mathbf{\Gamma}}^{11}_{ii,\mathrm{GAU}}$ is the limit of Eq. A.6 as $\mathbf{R}_{ij}$ approaches $\mathbf{0}$, namely

$$\hat{\mathbf{\Gamma}}^{11}_{ii,\mathrm{GAU}} = \lim_{\mathbf{R}_{ij}\to\mathbf{0}} \hat{\mathbf{\Gamma}}^{11}_{ij,\mathrm{GAU}} = \frac{1}{3}\sqrt{\frac{2}{\pi}}\sigma_i^{3/2}. \tag{A.7}$$

For the exponential-decay distribution, a similar analysis yields

$$\hat{\mathbf{\Gamma}}^{11}_{ij,\mathrm{EXP}} = \frac{-3\mathbf{R}_{ij}\otimes\mathbf{R}_{ij} + R_{ij}^2\mathbf{I}}{R_{ij}^5} + M_{ij}\mathbf{I} + N_{ij}\mathbf{R}_{ij}\otimes\mathbf{R}_{ij}, \tag{A.8}$$

where

$$M_{ij} = \begin{cases} e^{-\tau_i R_{ij}}\left[-\frac{\tau_j^4\tau_i}{2(\tau_i^2-\tau_j^2)^2}\frac{\tau_i}{R_{ij}} + \frac{\tau_j^6-3\tau_j^4\tau_i^2}{(\tau_i^2-\tau_j^2)^3}\frac{(\tau_i R_{ij}+1)}{R_{ij}^3}\right] \\ +e^{-\tau_j R_{ij}}\left[-\frac{\tau_i^4\tau_j}{2(\tau_j^2-\tau_i^2)^2}\frac{\tau_j}{R_{ij}} + \frac{\tau_i^6-3\tau_i^4\tau_j^2}{(\tau_j^2-\tau_i^2)^3}\frac{(\tau_j R_{ij}+1)}{R_{ij}^3}\right] & i\neq j, \tau_i\neq\tau_j \\ -e^{-\tau_i R_{ij}}\left(\frac{1}{R_{ij}^3} + \frac{\tau_i}{R_{ij}^2} + \frac{\tau_i^2}{2R_{ij}} + \frac{7\tau_i^3}{48} + \frac{\tau_i^4 R_{ij}}{48}\right) & i\neq j, \tau_i=\tau_j \end{cases} \tag{A.9}$$

and

$$N_{ij} = \begin{cases} e^{-\tau_i R_{ij}}\left[\frac{\tau_j^4\tau_i}{2(\tau_i^2-\tau_j^2)^2}\left(\frac{\tau_i^2}{R_{ij}^2}+\frac{\tau_i}{R_{ij}^3}\right) - \frac{\tau_j^6-3\tau_j^4\tau_i^2}{(\tau_i^2-\tau_j^2)^3}\left(\frac{\tau_i^2}{R_{ij}^3}+\frac{3\tau_i}{R_{ij}^4}+\frac{3}{R_{ij}^5}\right)\right] \\ +e^{-\tau_j R_{ij}}\left[\frac{\tau_i^4\tau_j}{2(\tau_j^2-\tau_i^2)^2}\left(\frac{\tau_j^2}{R_{ij}^2}+\frac{\tau_j}{R_{ij}^3}\right) - \frac{\tau_i^6-3\tau_i^4\tau_j^2}{(\tau_j^2-\tau_i^2)^3}\left(\frac{\tau_j^2}{R_{ij}^3}+\frac{3\tau_j}{R_{ij}^4}+\frac{3}{R_{ij}^5}\right)\right] & i\neq j, \tau_i\neq\tau_j \\ e^{-\tau_i R_{ij}}\left(\frac{3}{R_{ij}^5}+\frac{3\tau_i}{R_{ij}^4}+\frac{3\tau_i^2}{2R_{ij}^3}+\frac{\tau_i^3}{2R_{ij}^2}+\frac{\tau_i^4}{8R_{ij}}+\frac{\tau_i^5}{48}\right) & i\neq j, \tau_i=\tau_j. \end{cases} \tag{A.10}$$

In this case,

$$\hat{\mathbf{\Gamma}}^{11}_{ii,\mathrm{EXP}} = \lim_{\mathbf{R}_{ij}\to\mathbf{0}} \hat{\mathbf{\Gamma}}^{11}_{ij,\mathrm{EXP}} = \frac{1}{48}\tau_i^3. \tag{A.11}$$

Appendix B. Parametrization comparison.

Fig. B.3 shows a comparison of the sensitivity of calculated polarizabilities for sets of fullerenes and CNTs to the dipole distribution parameter τ_p. In order to bet-

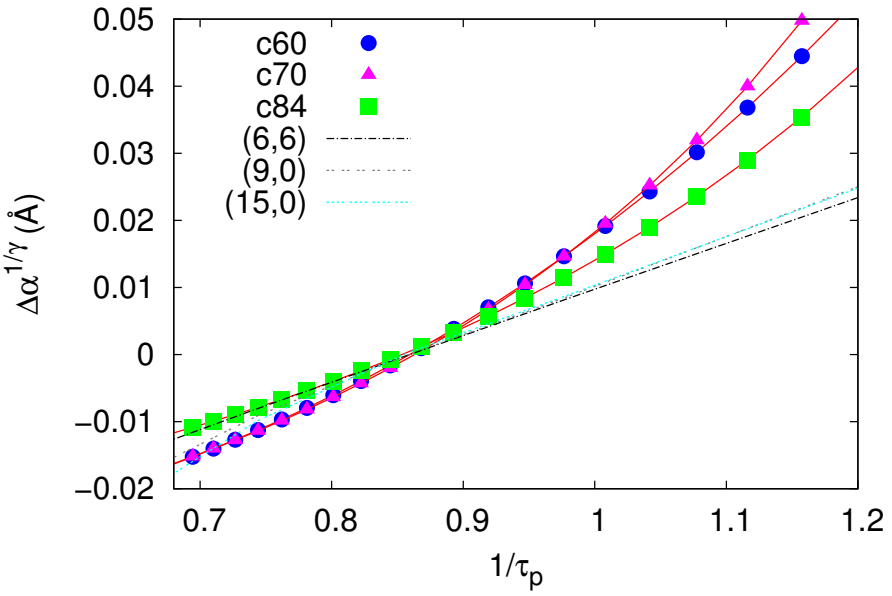

Figure B.3: Comparison of changes in rooted calculated polarizabilities ($\Delta\alpha^{1/\gamma}$) of a set of fullerenes ($\gamma = 3$) and carbon nanotubes ($\gamma = 2$) obtained from various dipole distribution parameter τ_p. The reference values are those obtained using $\tau_p = \tau_q (= 1.16)$.

ter compare these two family of systems, the calculated polarizabilities are rooted (cube rooted for fullerenes and square rooted for CNTs), so that $1/\tau_p$ and the rooted polarizabilities both have unit of a length. The CNTs then exhibit a consistent linear dependence with $1/\tau_p$ and fullerenes also exhibit a consistent but weakly nonlinear dependence of $1/\tau_p$, and these two sets show similar sensitivity towards the parameter τ_p.

Appendix C. Polarizabilities of monolayer graphene calculated using DFT.

Table C.2 gives polarizabilities of monolayer graphene calculated using the ab-initio DFT with *CRYSTAL14*[32], obtained using several different standard linear combination of atomic orbital basis sets. All calculations use a C-C bond length of 2.461 Å and 61 k points in the hexagonal Brillouin zone.

basis set [31]	LDA	PBE
6-21G	0.47	0.47
6-21G*	0.51	0.52
6-31d1G	0.59	0.60
TZVP	0.63	0.63

Table C.2: Perpendicular polarizability per unit cell ($Å^3$) of monolayer graphene using DFT calculated with different standard basis sets.

References

[1] D. Porezag, T. Frauenheim, T. Köhler, G. Seifert, R. Kaschner, Construction of tight-binding-like potentials on the basis of density-functional theory: Application to carbon, Phys. Rev. B 51 (1995) 12947.

[2] M. Elstner, D. Porezag, G. Jungnickel, J. Elsner, M. Haugk, T. Frauenheim, S. Suhai, G. Seifert, Self-consistent-charge density-functional tight-binding method for simulations of complex materials properties, Phys. Rev. B 58 (1998) 7260.

[3] J. Elsner, Surfaces and Extended Defects in Wurtzite GaN (PhD thesis), Universität-Gesamthochschule Paderborn, Paderborn, 1998.

[4] Z. Bodrog, B. Aradi, Possible improvements to the self-consistent-charges density-functional tight-binding method within the second order, Phys. Stat. Sol.(b) 249 (2012) 259–269.

[5] W. Kohn, L. J. Sham, Self-consistent equations including exchange and correlation effects, Phys. Rev. 140 (1965) A1133–A1138.

[6] P. Koskinen, V. Mäkinen, Density-functional tight-binding for beginners, Comp. Mater. Sci. 47 (2009) 237.

[7] H. Eschrig, I. Bergert, An optimized LCAO version for band structure calculations application to copper, Phys. Stat. Sol. (b) 90 (1978) 621.

[8] R. S. Mulliken, Electronic population analysis on LCAO-MO molecular wave functions. I, J. Chem. Phys. 23 (1955) 1833.

[9] B. Aradi, B. Hourahine, T. Frauenheim, DFTB+, a sparse matrix-based implementation of the DFTB method, J. Phys. Chem. A 111 (2007) 5678–5684.

[10] A. Mayer, Formulation in terms of normalized propagators of a charge-dipole model enabling the calculation of the polarization properties of fullerenes and carbon nanotubes, Phys. Rev. B 75 (2007) 045407.

[11] D. Jonsson, P. Norman, K. Ruud, H. Ågren, T. Helgaker, Electric and magnetic properties of fullerenes, J. Chem. Phys. 109 (1998) 572–577.

[12] M. van Faassen, L. Jensen, J. A. Berger, P. L. de Boeij, Size-scaling of the polarizability of tubular fullerenes investigated with time-dependent (current)-density-functional theory, Chem. Phys. Lett. 395 (2004) 274–278.

[13] R. R. Zope, The static dipole polarizability of C70 fullerene, J. Phys. B: At. Mol. Opt. Phys. 40 (2007) 3491.

[14] B. Kozinsky, N. Marzari, Static dielectric properties of carbon nanotubes from first principles, Phys. Rev. Lett. 96 (2006) 166801.

[15] E. Sohmen, J. Fink, W. Krätschmer, Electron energy-loss spectroscopy studies on C60 and C70 fullerite, Z. Physik B - Condensed Matter 86 (1992) 87–92.

[16] R. Antoine, P. Dugourd, D. Rayane, E. Benichou, M. Broyer, F. Chandezon, C. Guet, Direct measurement of the electric polarizability of isolated C60 molecules, J. Chem. Phys. 110 (1999) 9771–9772.

[17] I. Compagnon, R. Antoine, M. Broyer, P. Dugourd, J. Lermé, D. Rayane, Electric polarizability of isolated C70 molecules, Phys. Rev. A 64 (2001) 025201.

[18] A. F. Hebard, R. C. Haddon, R. M. Fleming, A. R. Kortan, Deposition and characterization of fullerene films, Appl. Phys. Lett. 59 (1991) 2109–2111.

[19] L. X. Benedict, S. G. Louie, M. L. Cohen, Static polarizabilities of single-wall carbon nanotubes, Phys. Rev. B 52 (1995) 8541–8549.

[20] G. Y. Guo, K. C. Chu, D.-s. Wang, C.-g. Duan, Linear and nonlinear optical properties of carbon nanotubes from first-principles calculations, Phys. Rev. B 69 (2004) 205416.

[21] G. Y. Guo, K. C. Chu, D.-s. Wang, C.-g. Duan, Static polarizability of carbon nanotubes: ab initio independent-particle calculations, Comp. Mater. Sci. 30 (2004) 269–273.

[22] E. N. Brothers, K. N. Kudin, G. E. Scuseria, C. W. Bauschlicher, Transverse polarizabilities of carbon nanotubes: A Hartree-Fock and density functional study, Phys. Rev. B 72 (2005) 033402.

[23] V. Lacivita, M. Rérat, R. Orlando, R. Dovesi, P. D'Arco, Longitudinal and transverse hyperpolarizabilities of carbon nanotubes: a computational investigation through the coupled-perturbed Hartree-Fock/Kohn-Sham scheme, Theor. Chem. Acc. 135 (2016) 1–13.

[24] R. Demichelis, Y. Noël, P. D'Arco, M. Rèrat, C. M. Zicovich-Wilson, R. Dovesi, Properties of carbon nanotubes: An ab initio study using large gaussian basis sets and various dft functionals, J. Phys. Chem. C 115 (2011) 8876–8885.

[25] M. Boleininger, A. A. Guilbert, A. P. Horsfield, Gaussian polarizable-ion tight binding, J. Chem. Phys 145 (2016) 144103.

[26] T. J. Giese, D. M. York, Density-functional expansion methods: grand challenges, Theor. Chem. Acc. 131 (2012) 1145.

[27] S. Kaminski, T. J. Giese, M. Gaus, D. M. York, M. Elstner, Extended polarization in third-order scc-dftb from chemical-potential equalization, J. Phys. Chem. A 116 (2012) 9131–9141. PMID: 22894819.

[28] A. S. Christensen, M. Elstner, Q. Cui, Improving intermolecular interactions in dftb3 using extended polarization from chemical-potential equalization, J. Chem. Phys 143 (2015) 084123.

[29] C. Iftner, A. Simon, K. Korchagina, M. Rapacioli, F. Spiegelman, A density functional tight binding/force field approach to the interaction of molecules with rare gas clusters: Application to $(C6H6)^{+/0}$ Ar_n clusters, J. Chem. Phys 140 (2014) 034301.

[30] M. Gaus, Q. Cui, M. Elstner, DFTB3: Extension of the self-consistent-charge density-functional tight-binding method (SCC-DFTB), J. Chem. Theory Comput. 7 (2011) 931–948.

[31] K. L. Schuchardt, B. T. Didier, T. Elsethagen, L. Sun, V. Gurumoorthi, J. Chase, J. Li, T. L. Windus, Basis set exchange: A community database for computational sciences, J. Chem. Inf. Model. 47 (2007) 1045–1052.

[32] R. Dovesi, R. Orlando, A. Erba, C. M. Zicovich-Wilson, B. Civalleri, S. Casassa, L. Maschio, M. Ferrabone, M. De La Pierre, P. D'Arco, Y. Noël, M. Cauà, M. Rérat, B. Kirtman, CRYSTAL14: A program for the ab initio investigation of crystalline solids, Int. J. Quantum. Chem. 114 (2014) 1287–1317.